Annals of Anatomy 251 (2024) 152168

Contents lists available at ScienceDirect

Annals of Anatomy

journal homepage: www.elsevier.com/locate/aanat

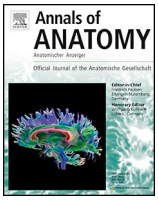

Clinical anatomy of the spina musculi recti lateralis: A frequently overlooked variation of the greater wing of the sphenoid

Denise Bonente [a,b], Virginia Barone [a], Vitaliano Francesco Muzii [c], Sara Ottolenghi [d], Miriam Durante [a], Sandra Bracco [e], Claudio Nicoletti [a], Eugenio Bertelli [a,*]

[a] Dept. of Molecular and Developmental Medicine, University of Siena, Siena, Italy
[b] Dept of Life Sciences, University of Siena, Siena, Italy
[c] Dept of Medicine, Surgery and Neuroscience, University of Siena, Siena, Italy
[d] Radiology Department, Santa Corona Hospital, Pietra Ligure, Italy
[e] Neuroradiologia Interventistica, Ospedale S. Maria delle Scotte-University Hospital, Siena, Italy

ARTICLE INFO

Keywords:
Orbit
Neuronavigation
Annulus of Zinn
Superior orbital fissure syndrome
Orbital apex syndrome

ABSTRACT

Background: The spina musculi recti lateralis (SMRL) is often visible along the lateral rim of the superior orbital fissure (SOF). Aim of this study is to characterize SMRL morphology and topography relative to known bony landmarks.

Methods: Orbits from 291 adult dry skulls and from 60 CT scans were analyzed to measure the distance between the SMRL and the SOF or the inferior orbital fissures (IOF) as well as its height, width and orientation. Processes other than SMRLs were also recorded. Fetal skulls were observed for comparison with adult samples.

Results: Forty-one per cent of orbits on dry skulls and 43.3% by CT showed an SMRL. Additional 32.9% of orbits on dry skulls had processes with a different shape. On average, SMRL were orientated almost along the transverse plane and showed implant bases as wide as 141.9° or as narrow as 36.8°. SMRLs were close to the infero-posterior angle of the orbital plate of the sphenoid, 1.21 ± 0.84 mm in front of the SOF, 5.8 ± 1.9 mm above the IOF and 12 ± 2.3 mm from the anterior end of the SOF. They were 1.58 ± 0.64 mm high and did not show any age or sex-related prevalence. By CT, the SMRL appeared as the insertion site for the lateral rectus, tendinous ring and, sometimes, inferior rectus.

Conclusions: The SMRL is a process of the sphenoidal orbital plate rather than of the SOF. It is also a reliable landmark for the insertion of the tendinous ring and lateral rectus. Orbital surgeons should be aware of this common variant of the orbital apex.

1. Introduction

It is often taken for granted that orbit osteology has been extensively explored and that little remains to be studied. This is true only in part as some structures, though known for a long time, have been merely enlisted among the anatomical landmarks without ever being adequately characterized. For instance, until recently the orbitomeningeal and metoptic canals had not been studied in detail (Bertelli, 2014; Macchi et al., 2016) and a novel rare canal opening into the orbit had never been acknowledged (Bertelli and Regoli, 2014). The spina musculi recti lateralis (SMRL), a bony process of the greater wing of the sphenoid projecting into the orbital apex, is certainly among the structures of the orbit that still awaits a proper characterization. The orbital apex has a conical shape with the apex of the cone pointing backward approximatively toward the optic strut and the forward-directed base that continues seamlessly into the remaining of the orbit. The bony walls incompletely surround the orbital apex as they are provided with openings crossed by nerves and vessels leaving or reaching the orbit (Regoli and Bertelli, 2017). The optic canal, located upward and medially to the optic strut, transmits the optic nerve and the ophthalmic artery. Downward, the floor of the orbital apex is partially absent as the orbital space continues with the vertically–oriented pterygopalatine fossa. The superior orbital fissure (SOF), located laterally to the optic strut and extending upward and forward, gives passage to the nasociliary, trochlear, frontal, lacrimal and abducens nerves, the superior and inferior divisions of the oculomotor nerve, the sympathetic and long

* Correspondence to: Dept. of Molecular and Developmental Medicine, University of Siena, Via Aldo Moro, Siena I-53100, Italy
E-mail address: eugenio.bertelli@unisi.it (E. Bertelli).

https://doi.org/10.1016/j.aanat.2023.152168
Received 7 August 2023; Received in revised form 20 September 2023; Accepted 9 October 2023
Available online 14 October 2023

roots of the ciliary ganglion and the superior ophthalmic vein (Lang, 1983). Less frequently, the deep and superficial recurrent ophthalmic arteries, the meningophthalmic artery, the inferior ophthalmic vein and even a second ophthalmic artery can also traverse the fissure (Bracco et al., 2016; Bertelli et al., 2017., Bertelli, 2019). By looking at this long list, it is quite evident why surgery of the orbital apex is particularly challenging. Any item that occupies room in such a narrow and crowded region can make surgery even more testing.

The SMRL sometime extends into the orbital apex giving insertion to one head of the lateral rectus muscle (Lang, 1983; Bron et al., 2001). It is reported as located along the lower margin of the SOF at the junction of the wider posterior and the narrower anterior portions of the fissure (Lang, 1983; Bron et al., 2001; Snell and Lemp, 2016). Apart from this generic description, the only account on the subject is a short note reporting anatomic frequency and a certain variability in shape (Bisaria et al., 1996). In order to supply useful information to the orbital surgeons, we specified topographic and morphologic features of the SMRL on dry skulls and we analyzed retrospectively a series of computed tomographies (CT) to identify anatomical structures inserting into the spine.

2. Material and methods

2.1. Anatomical samples

For this investigation we employed the collection of dry adult and fetal human skulls housed at the Anatomical Museum of the University of Siena (Department of Medicine, Surgery and Neurosciences) (Bertelli, 2014). From this collection, we selected 291 skulls of known sex and/or age. As few orbits were spoiled, we studied 568 orbits of individuals with an average age of 58.2±16.5 years (range between 16 and 92 years) overall. Sex was known for 507 orbits (282 male orbits, 225 female orbits). The collection of fetal skulls consisted of 360 samples whose age was estimated according to the biparietal diameter (Snijders and Nicolaides, 1994). Fetal skulls were included only to document paradigmatic aspects of SMRL development.

Adult skulls were examined to look for the SMRL as a pointed eminence raising from the orbital plate of the sphenoid. Whenever an SMRL was found, the following measures were taken with the help of calipers and graduated scales: distance between the base of the spine and the inferior orbital fissure (IOF) (a in Fig. 1B), distance between the spine apex and the IOF (b in Fig. 1B), distance between the base of the spine and the anterior end of the SOF (c in Fig. 1B), distance between the spine apex and the anterior end of the SOF (d in Fig. 1B). The length of the spine (a in Fig. 1C) and the distance between the base of the spine and the SOF rim (b in Fig. 1C) were also recorded. Finally, in order to define SMRL width and orientation, the angle encompassed between the spine margins (Fig. 1D) and the angle comprised between the spine axis, defined as the bisector of the previous angle, and the transverse plane (Fig. 1E) were measured using ImageJ 1.53 t software (NIH, USA).

Other types of processes (tubercles, tongue-like processes, plaques, various thickenings) could be also observed replacing or doubling the SMRL. For tubercles, defined as small stubby and chamfered eminences with a wide base (Fig. 2A), we recorded the distances between the base and the IOF (a in Fig. 2B), the SOF anterior end (b in Fig. 2B), and the SOF rim (c in Fig. 2B). Tongue-like processes (also lingulae) were flattened prominences with a wide base and an inclined rounded apex (like a drop of viscous fluid on a vertical surface) (Fig. 2C). For them, we took the same measures recorded for the SMRL (Fig. 2D). For plaques, defined as focal thickenings of the orbital plate with clear step-like boundaries

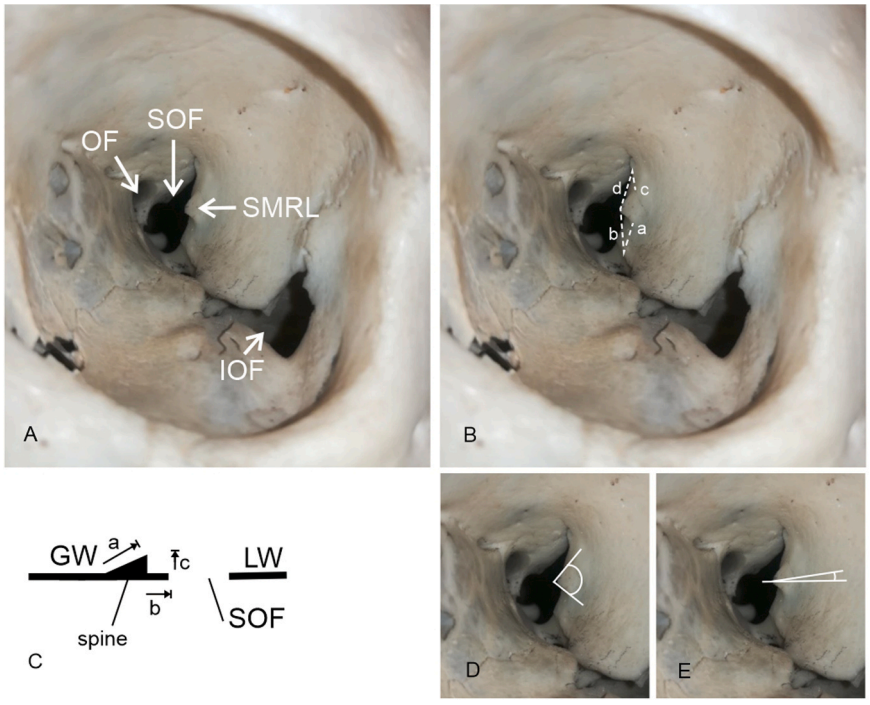

Fig. 1. Morphometric evaluation of the SMRL. A) Example of an SMRL. OF = Optic foramen; SOF = superior orbital fissure; IOF = inferior orbital fissure. B) Measurements taken to precise the position on the orbital plate of the sphenoid of the spine shown in A: a) distance between the base of the spine and the IOF; b) distance between the spine apex and the IOF; c) distance between the base of the spine and the anterior end of the SOF; d) distance between the spine apex and the anterior end of the SOF. C) Sketch of an axial section passing through the SOF and intersecting the greater wing (GW) and the lesser wing (LW) of the sphenoid. The spine is represented by a pointed thickening of the GW. The sketch illustrates three additional measurements that were taken: a) length of the spine; b) distance between the spine and the SOF margin; c) height of the spine on the orbital plate of the sphenoid (this measure was taken only by CT). D) The size of the base of the spine shown in A was evaluated assessing the angle formed by the spine margins. E) The orientation of the spine shown in A was assessed measuring the angle encompassed between the transverse plane and the spine axis (the bisector of the angle shown in D). In the example the orientation of the SMRL is slightly downward, very close to the transverse plane.

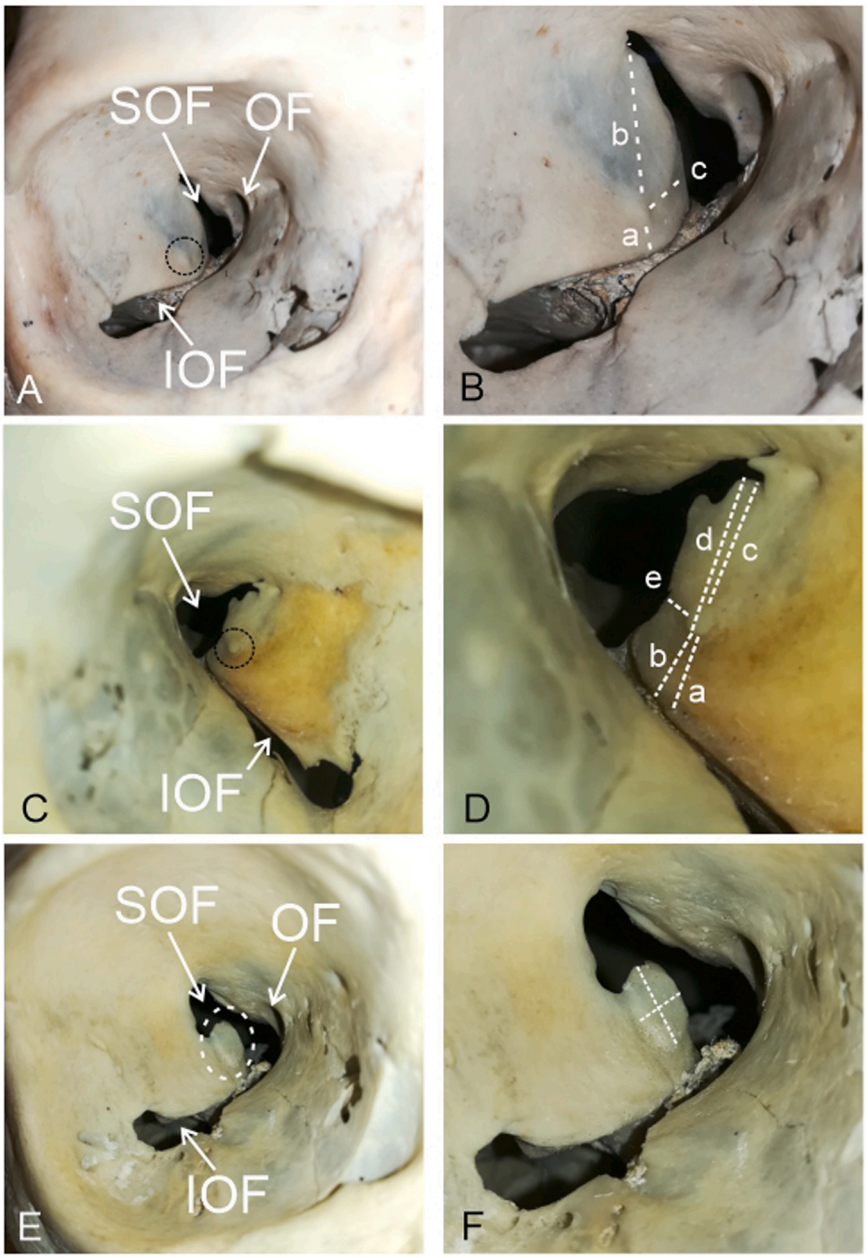

Fig. 2. Morphometric evaluation of small bony processes of the sphenoid orbital plate other than the SMRL. A) Tubercle. OF = Optic foramen; SOF = superior orbital fissure; IOF = inferior orbital fissure. B) Measurements taken to precise the position on the orbital plate of the sphenoid of the tubercle shown in A: a) distance between the tubercle margin and the IOF; b) distance between the tubercle margin and the anterior end of the SOF; c) distance between the tubercle margin and the SOF rim. C) Tongue-like processes. SOF = superior orbital fissure; IOF = inferior orbital fissure. D) Measurements taken to precise the position of the lingula shown in C on the orbital plate of the sphenoid: a) distance between the lingula apex and the IOF; b) distance between the lingula base and the IOF; c) distance between the lingula base and the anterior end of the SOF; d) distance between the lingula apex and the anterior end of the SOF; e) distance between the lingula and the SOF margin. E) Plaque. OF = Optic foramen; SOF = superior orbital fissure; IOF = inferior orbital fissure. F) Measurements taken to characterize the size of the plaque shown in E.

(Fig. 2E), we measured major and minor axes (Fig. 2F). For other thickenings lacking well-defined margins, we recorded only their presence without taking any measure. Observations were carried out independently by two distinct investigators (D.B and M.D.). The identification carried out by the two observers of SMRLs and plaques was almost always concordant. The assignment of other processes (tubercles and lingulae) to one specific type was sometime less obvious. At any rate, when disagreements raised, the senior author (E.B.) had the final word.

Statistical analysis was carried out to verify if our findings could be sex- or age-related. In the first case, we applied the Chi squared test with Yates' correction. In the second case, we clustered our results by age groups which were compared applying the Chi squared test. In both cases, a p value ≤ 0.05 was considered significant.

2.2. Computed tomography (CT)

As the study on CT was retrospective, we did not obtain informed consent from patients. Sixty patients (120 orbits) were randomly selected (33 females and 27 males with an average age of 58.9 $\pm$ 18.2 years) from the archives of the Unit of Interventional Neuroradiology (Siena). The subjects had undergone CT examination for several reasons

including trauma, nasal polyposis, sinusitis and tumors. Exclusion criteria comprised all cases in which the above-mentioned pathologies somehow involved the orbital apex (e.g. tumors and serious traumatic injuries). CT scans were obtained with a GE Lighspeed VCT 64 slices (General Electric Healthcare Italia, Milano, Italy). Spiral scanning was performed at 140 kVp with "smart mA" function for thickness of 0.625 mm or 1.250 mm. Post-processing of the CT scans was carried out with RadiAnt DICOM viewer (version 2022.1.1) software. 3D reconstructions were generated and reviewed with the same software. Two distinct investigators (D.B and M.D.) carried out evaluations that were consistent in 100% of cases as far as the SMRL was concerned. Some problems could arise for the identification of other processes (tubercles, plaques or other thickenings). When this occurred, the senior author (E.B.) and the senior radiologist (S.B.) discussed the matter finding always an agreement for the definitive assignment of the process to the proper category. The same measurements taken on dry skulls were also recorded on CT scans. In addition, we also measured the maximal height that the SMRL reached over the orbital plate of the sphenoid (a in Fig. 1C).

3. Results

3.1. SMRL frequency

Overall, the observation of 568 orbits on dry skulls showed that 420 of them (73.94%) were associated with a bony process. Of these, 233 orbits (55.48% of the orbits with a bony process and 41.02% of all examined orbits) were provided with an SMRL whereas the remaining 187 orbits (44.52% of the orbits with a bony process and 32.92% of all examined orbits) showed other processes including lingulae, tubercles, plaques and other local thickenings. The SMRL was bilateral in 77 skulls (26.46%) whereas was located only on one side in 79 skulls (27.15%). Of these, 49 SMRLs (62.03%) were on the left orbit and 30 (37.97%) on the right orbit with a significant left prevalence ($p < 0.01$). CT demonstrated orbits associated with bony processes of the sphenoid in a lower number of cases. In such conditions we could detect some type of processes only in 61 orbits out of 120 (50.84%) including 52 orbits with the SMRL whose frequency (43.3% of orbits), however, roughly matched that observed on dry skulls. Overall, therefore, CT resulted less sensitive to detect processes that were much smaller than SMRLs. The SMRL was present in 34 individuals (56.67%) and it was bilateral in 18 subjects (30%). In the remaining 16 orbits (26.67%) the SMRL was found only on one side. When unilateral, the SMRL was observed on the left orbit in 12 cases (75%) and on the right orbit in 4 cases (25%) with a significant left prevalence ($p < 0.01$).

3.2. General morphology of SMRL

SMRLs showed remarkable morphologic variations ranging from triangular acuminated spines with a base of implant of variable size, to spines with a smoothened or truncated apex (Fig. 3). We also noted that in nine orbits the SMRL could be double (3.86% of the orbits associated with SMRLs) and occasionally even triple (Fig. 3). Morphologic features of the SMRL that could be quantified are summarized in Table 1. The width of the base, for instance, could be objectively assessed as the angle encompassed by the spine margins. The average value of the angle was 94.04% ± 20.21° with a range comprised between 36.87° (narrow spines) to 141.91° (wide spines). As testified by the average value, the greater part of the spines, 132 out of 233 (56.65%), were large enough to form obtuse angles (wide implant base) whereas acute angles (narrow implant base) were characteristic of 101 spines (43.35%). SMRL orientation could have negative values, corresponding to spines pointing upward, or positive values for spines pointing downward. The average angle of 1.43° ± 14.79° showed that in most cases spine orientation was very close to the transverse axis. However, the range of the inclination degree on the transverse plane was comprised between −90° and 66.26° (Fig. 3). Considering also orbits with double and triple spines, we observed negative values in 112 cases out of 244 SMRLs (45.90%) and positive values in the remaining 132 cases (54.10%).

Results obtained by CT were similar to those assessed by direct measurements (Table 1, Fig. 3). The only difference regarded the orientation that, though still close to the transverse plane, on average pointed slightly upward (angle with the transverse plane: −7.52 ±13.16). Indeed, prevalence was in favor of SMRLs pointing upward, with 40 orbits (76.92%) having angles with negative values and 12 orbits (13.08%) having angles with positive values. By CT, we could also make a reliable evaluation of the maximal height that the SMRL reached over the orbital plate (1.58 ± 0.64 mm; range 0.8–3.5 mm).

3.3. Topography of the SMRL

Dry skulls gave us the opportunity to precise the position of the SMRL with respect to known bony landmarks (Table 1). Distance between the spine and the SOF rim was comprised between 0 and 7.5 mm. A null distance, corresponding to a spine located exactly along the SOF margin, occurred in 30 cases (12.9% of the observed spines). This is the position usually described for the SMRL (Lang, 1983; Bron et al., 2001) but most SMRLs (87,1%) were indeed placed in a more advanced position, between 0.5 and 7 mm from the SOF margin (average distance 1.21 ± 0.84 mm). This measurement could not be recorded in 69 skulls because the intact cranial vault did not allow access to the spine from behind. Other measures that were taken (distances between base or apex of the SMRL and the IOF or the anterior end of the SOF) are summarized in Table 1. Data from CT almost matched those of dry skulls (Table 1), with the only difference regarding the distance between the SMRL and the anterior end of the SOF which resulted considerably shorter.

3.4. Age and sex-related differences

The sex of the orbits provided with an SMRL was known in 211 cases. SMRL was present in 113 male orbits (53.55%) and in 98 female orbits (46.45%). Orbits containing an SMRL and studied by CT belonged to males in 22 cases (42.31%) and to females in 30 cases (57.69%). Statistical analysis did not demonstrate any significative sex-related difference in SMRL frequency. Orbits associated with an SMRL belonged to individuals of known age in 154 cases (average 57.2 ± 16.38 years; range between 16 and 92 years-old). Cases of SMRLs studied by CT belonged to 59.85 ± 19.60 years-old individuals. A dispersion graph aimed to verify whether the SMRL grows with aging, did not demonstrate any obvious correlation between spine length and age (data not shown).

3.5. Other bony processes

Bony processes other than SMRLs could be observed roughly on the same place of the SMRL or in close proximity to it. According to their shape they could be distinguished as tubercles, tongue-like, plaques, and local thickenings (see 2.1). Tubercles were found in only 20 orbits out of 568 (3.52%). A similar frequency, 5 orbits out of 120 (4.16%), was assessed by CT. Distances of tubercles from orbital bony landmarks are summarized in Table 2. Tongue-like processes were observed in 25 orbits (4.4%). Distances of the lingulae from orbital bony landmarks are also summarized in Table 2.

Plaques could be seen in 46 orbits (8.1%). Their morphology varied from small processes located close to the SOF rim, to very prominent structures often with a quadrangular shape that could have a pointed extremity (Fig. 4). In the latter case, the only feature distinguishing plaques from an SMRLs was their clear-cut boundaries. The longer and the shorter axes of the plaques were 6.95 ± 2.66 mm and 4.39 ±2.07 mm respectively. CT demonstrated plaques and tongue-like processes only in three orbits (2.5%) (Fig. 4).

A thickening of the orbital plate raising progressively from the front

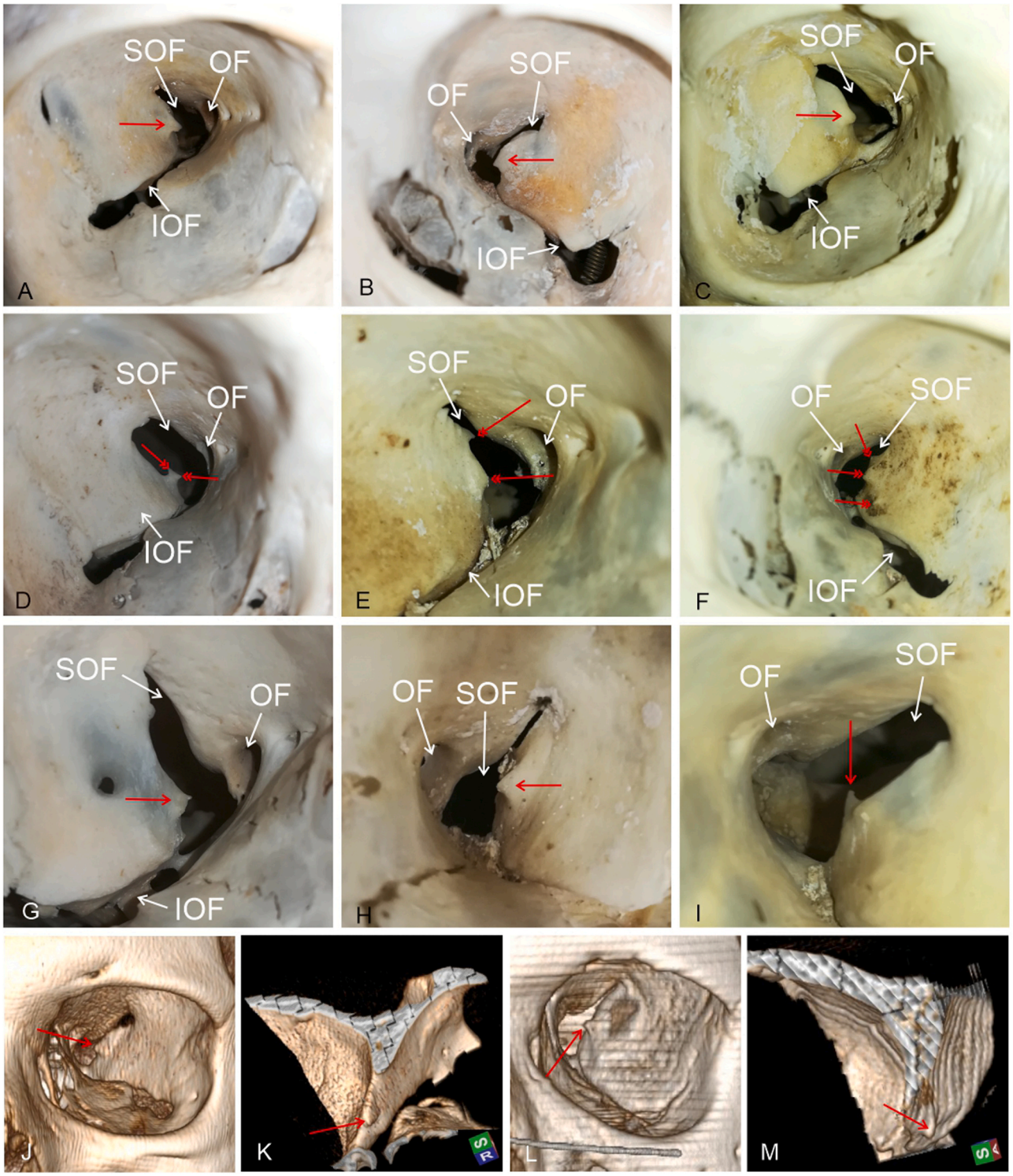

Fig. 3. Morphologic variations of SMRLs (red arrows). OF = Optic foramen; SOF = superior orbital fissure; IOF = inferior orbital fissure. A) SMRL with a narrow base. B) SMRL with a wide base. C) SMRL with a smoothened point. D) Double SMRL (double-pointed red arrows) arising as a single process from the orbital plate of the sphenoid. E) Two independent spines (double-pointed red arrows) in the same orbit. F) Three SMRLs (double-pointed red arrows) simultaneously present in the same orbit. G) SMRL arising from the SOF margin; H) SMRL arising 3 mm in front of the SOF, plainly from the orbital plate of the sphenoid greater wing; I) A very peculiar SMRL points upward (−90° from the transverse plane). A second SMRL is also visible just in front of the highlighted spine; J) SMRL arising very close to the SOF margin as seen by 3D rendering of CT scans; K) The same SMRL in J as seen after clipping away most of the skull and leaving the orbital plate of the sphenoid and part of the sphenotemporal fossa. Oblique view from medially, above and behind. L) A 2.3 mm high SMRL arising 1.6 mm in front of the SOF margin as seen by 3D rendering of CT scans; M) The same SMRL in L as seen after clipping away most of the skull and leaving the orbital plate of the sphenoid and part of the sphenotemporal fossa. Oblique view from above, medially and behind.

Table 1
SMRL size and orientation and SMRL topography. To assess SMRL size, measures, expressed in mm, were taken for spine length, height and base width. Orientation was measured as the angle encompassed by the spine axis and the transverse plane (see Section 2.1). Measures were taken on CT scans from live subjects or on dry skulls. ND = Not Determined. SMRL topography was assessed by measuring the distance, expressed in mm, between the spine and the bony landmarks listed in the left column (see Section 2.1). Measures were taken on CT scans from live subjects and on dry skulls.

SMRL Morphologic Features						
	Average		Maximum		Minimum	
	Dry skulls	CT	Dry Skulls	CT	Dry Skulls	CT
Length	3.27 ± 1.28	3.42 ± 1.23	7	7.3	0.5	1.4
Height	ND	1.58 ± 0.64	ND	0.8	ND	3.5
Base width	94.04 ±20.21	102.96 ±25.17	141.91	142	36.87	23
Orientation	1.43° ±14.79°	-7.52° ±13.16°	66.26°	27°	-90°	-40°

SMRL Topography						
	Average		Maximum		Minimum	
	Dry skulls	CT	Dry Skulls	CT	Dry Skulls	CT
SMRL base-SOF anterior end	8.1 ±0.2.6	6.2 ±0.2.7	14	10.3	0	1
SMRL apex-SOF anterior end	12±2.3	9.4±3.0	18	14.1	1	2.7
SMRL base-SOF lower margin	1.2±0.8	1.0±0.9	7	3.8	0.5	0
SMRL base-IOF	5.8±1.9	4.6±1.7	16	9.7	1	2
SMRL apex-IOF	6.3±2.3	6.4±1.8	19	11.9	1	3.6

Table 2
Topography of tubercles and lingulae. Tubercles and lingulae topography were assessed by measuring the distance, expressed in mm, between their rising from the bony plate and the bony landmarks listed in the left column (see Section 2.1). Measures were taken on dry skulls and on CT scans from live subjects with the exception of lingulae which were seen only on dry skulls.

Tubercle Topography						
	Average		Maximum		Minimum	
	Dry skulls	CT	Dry Skulls	CT	Dry Skulls	CT
Tubercle base-SOF anterior end	9.88 ±2.83	10.0 ±2.16	14	13.6	5	7.7
Tubercle base-SOF lower margin	4.66 ±3.38	5.75 ±1.44	11	7.6	3	3.7
Tubercle base-IOF	6±2.43	4.77 ±2.94	10	7	2	0
Tongue-like processes (lingulae) Topography						
	Average		Maximum		Minimum	
	Dry skulls	CT	Dry Skulls	CT	Dry Skulls	CT
Lingula base-SOF anterior end	12.32 ±2.36	ND	16	ND	8	ND
Lingula apex-SOF anterior end	14.36 ±2.10	ND	18	ND	10	ND
Lingula base-SOF lower margin	8.68 ±2.91	ND	15	ND	2	ND
Lingula base-IOF	4.68 ±1.47	ND	8	ND	2	ND
Lingula apex-IOF	5.76 ±1.64	ND	9	ND	3	ND

backward could be observed on dry skulls in 110 cases (19.36% of orbits). They resembled SMRLs with large implant bases, but they were devoid of any pointed end. Finally, in additional 88 orbits (15.49%) the thickenings assumed the shape of bony crests with a linear or semicircular profile. Crest-like thickenings were associated with lingulae in 13 cases. Similar thickenings were detectable on CT scans only in two orbits (1.6%).

Interestingly, a small tubercle raising from the base of the optic strut could be seen in 55 of the orbits bearing an SMRL (23.6%). Its position, opposite to the spine, suggests the possible site of insertion of ligamentous structures crossing the SOF from the SMRL (Fig. 4F).

3.6. Fetal skulls

As for adults, the SMRL was an inconstant feature also in fetuses. In our collection a prominent SMRL could be detected in a variety of skulls of the apparent gestational age of 32–34 weeks (Fig. 5). However, we could also find cases of SMRLs in younger skulls, of the apparent gestational age of 28 weeks (Fig. 5B). Though we could not find good examples of SMRL in fetuses younger than 28 weeks, judging by the size of SMRLs at the 28th week, we can assume that SMRLs development starts even at an earlier stage of gestation. Interestingly, one skull of the apparent gestational age of 32 weeks was still provided with a remnant of fibrous tissue crossing the SOF from the SMRL to the base of the optic strut approximatively at the same level of the tubercle observed in adult skulls (Fig. 5D).

3.7. Insertions

An attempt to identify anatomical structures inserting into the SMRL has been carried out on CT scans by 3D multiplanar reconstruction (MPR) when spines were large enough and protruded into the orbital cavity. As expected, the insertion of part of the lateral rectus was a constant feature. However, in some cases even part of the inferior rectus seemed to insert into the SMRL (Fig. 6). A more convincing observation regarded a constant radiopaque stripe of tissue that arose from the SMRL, almost as a continuation of the lateral rectus, and inserted into the base of the optic strut infero-medial to the optic foramen. We interpreted this band of tissue as the lower part of the annulus of Zinn since it is the only known structure that crosses transversely the SOF (Fig. 6). It is suggestive how its course matches that of the fibrous remnant observed in the fetal skull of Fig. 5D.

4. Discussion

The SMRL is a bony projection that has been known for a long time (Thane, 1893). Nevertheless, its precise position and morphologic features have never been studied in detail. To our knowledge, its frequency has been determined only once (Bisaria et al., 1996) including in the definition of SMRL also other bony processes whose shape was not spiny (tongue-shape, quadrangular, plate, tubercle). Previous assessment of the anatomic frequency of all these bony processes (62.7%) was not much different from our estimation (73%) which also acknowledged additional shapes (i.e. crest-like thickenings). A limitation of our study is that the assignment of a bony process to one type rather than another is somehow subjective. Yet, as borderline cases were very few, we do not believe that their shift from one category to another would substantially change our statistics.

In addition to confirming previous observations (Bisaria et al., 1996), we could precise morphometric and topographic characteristics of SMRLs and of other bony processes present in the same area. As we have seen, SMRLs projected into the orbit in variable ways. Only the longest and highest SMRLs probably acquire clinical relevance. On dry skulls, SMRLs longer than 5 mm were present in 54 cases (9.5% of all examined orbits). Furthermore, nine orbits out of 120 (7.5%) had spines higher than 2 mm as to say that they are provided with a bony process that can significantly reduce the narrow room of the orbital apex. The orbital apex is a region where two largely overlapping compressive disorders, SOF and orbital apex syndromes, can develop. The orbital apex

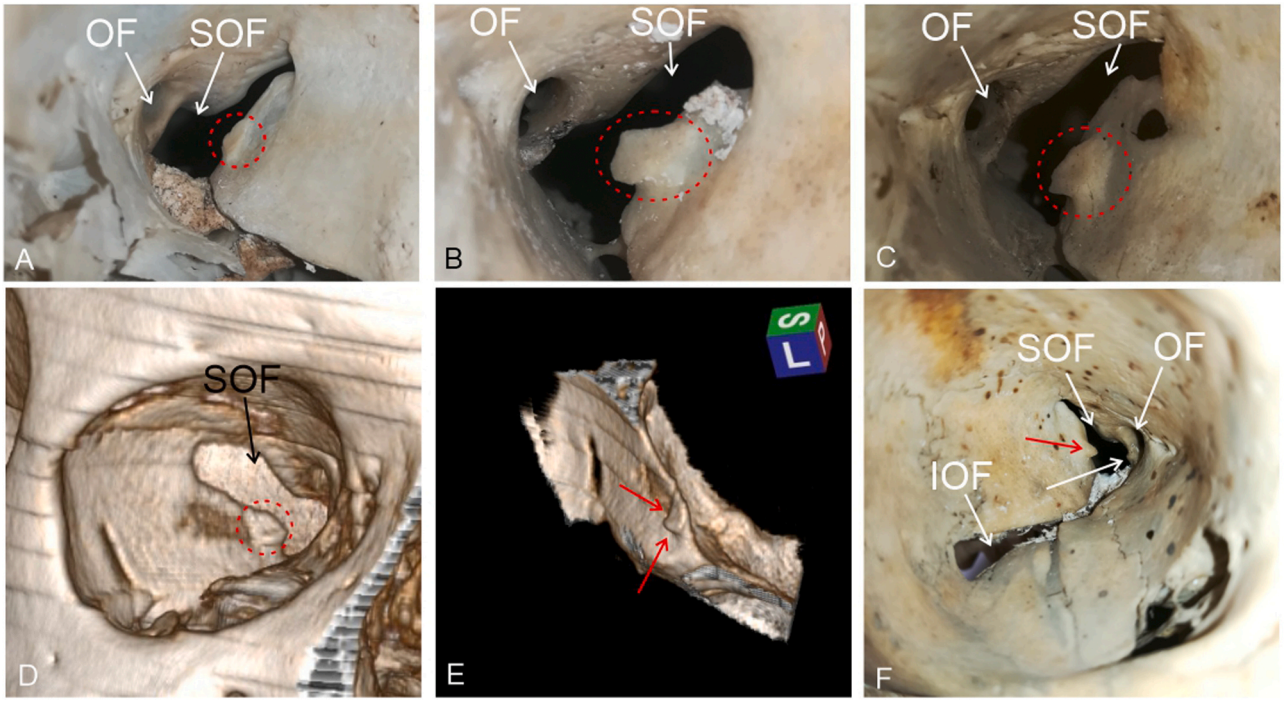

Fig. 4. Morphologic variation of the plaques; tubercles on the optic strut opposite to the SMRL. OF = Optic foramen; SOF = superior orbital fissure; IOF = inferior orbital fissure A) Small plaque (within the red framed area) placed just in front of the SOF; B) Quadrangular large plaque (within the red framed area) projects for several millimeters into the orbit; C) Plaque shaped like an SMRL with clear step-like boundaries (within the red framed area). It projects for several millimeters into the orbit; D) 3D-rendering of a CT scan with a plaque (within the red framed area) very similar to example in C; E) The same plaque in D as seen after clipping away most of the skull and leaving the orbital plate of the sphenoid. The oblique view from above, medially and behind gives a better appreciation of the step-like boundaries of the plaque (red arrows); F) An SMRL (red arrow) is associated with a small tubercle raising from the base of the optic strut (white unlabeled arrow).

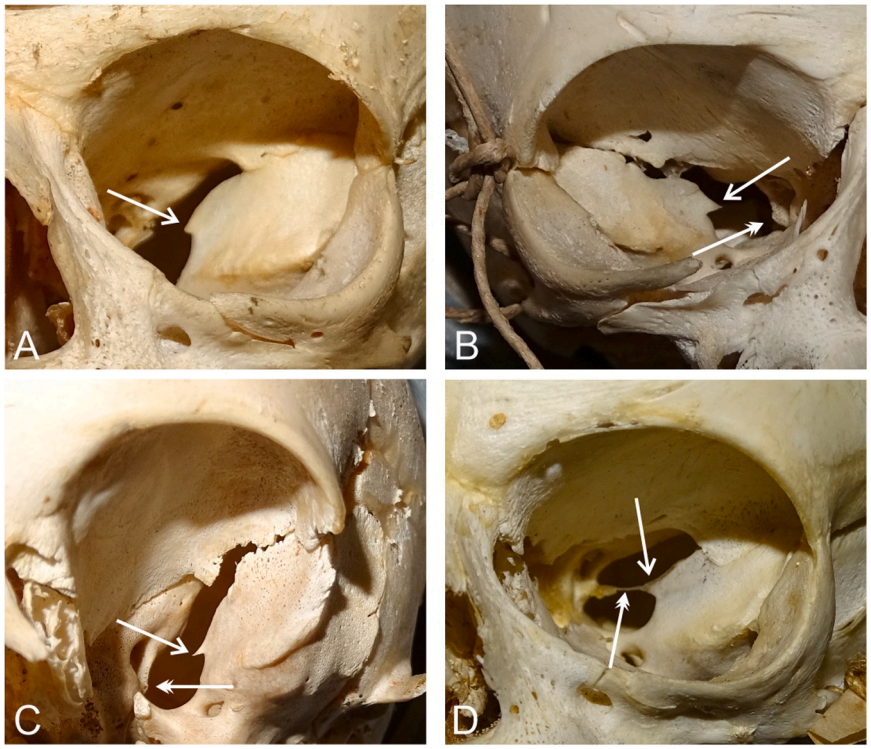

Fig. 5. SMRLs in fetal skulls. A) An SMRL in a skull of the apparent gestational age of 33 weeks shows remarkable morphologic similarities with the SMRL shown in Fig. 3B; B) An extremely pointed SMRL (arrow) in a skull of the apparent gestational age of 28 weeks. Note the small tubercle (double-pointed arrow) at the base of the optic strut. C) An extremely pointed SMRL (arrow) in a skull of the apparent gestational age of 33 weeks. Once again, note the small tubercle (double-pointed arrow) at the base of the optic strut; the zygomatic and maxillary bones have been disarticulated. D) An SMRL (arrow) in a skull of the apparent gestational age of 32 weeks. A remnant band of fibrous tissue crosses the SOF to insert into the base of the optic strut.

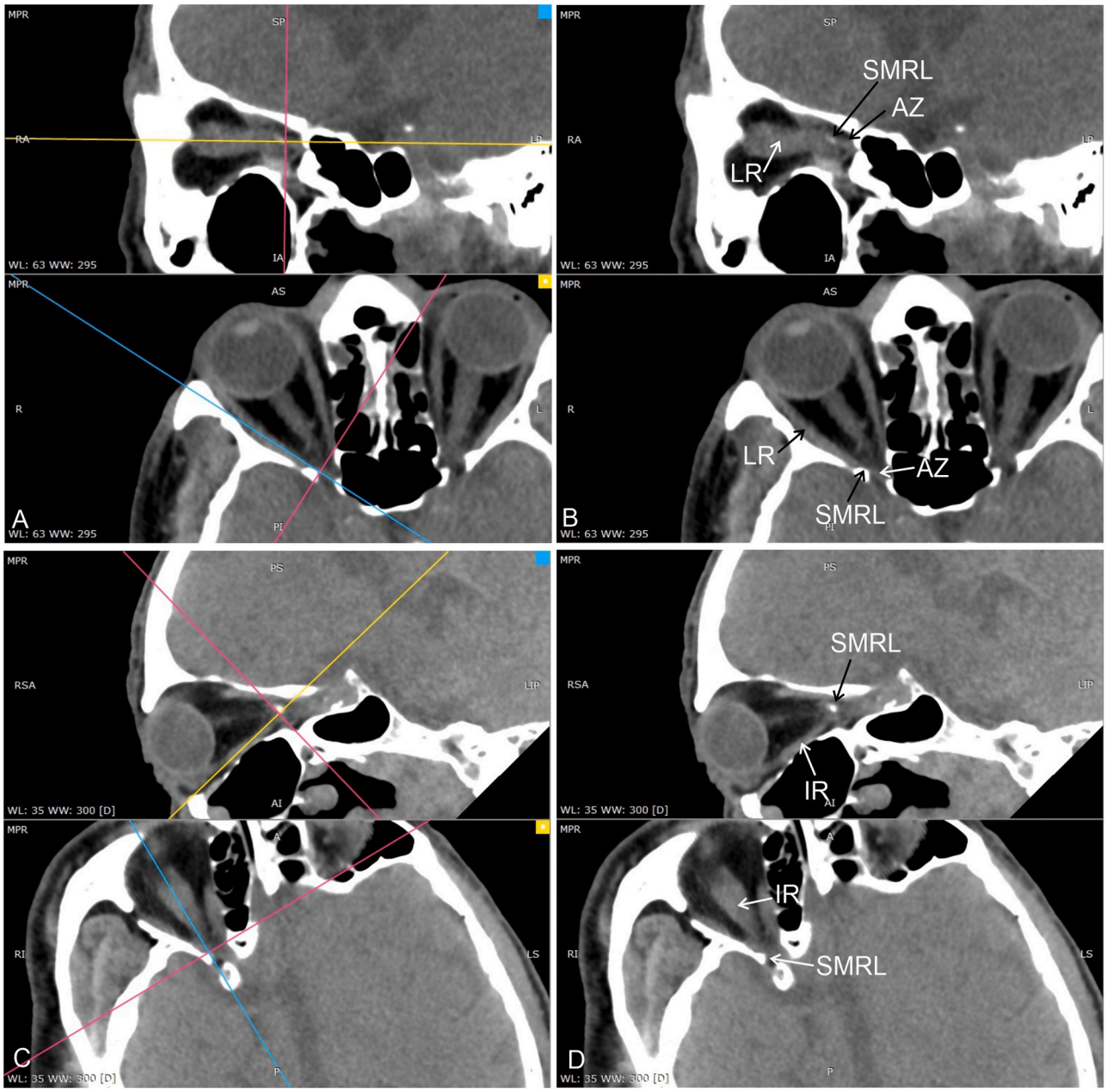

Fig. 6. 3D multiplanar reconstruction of one orbit with an SMRL. A) Two spatial planes (blue and yellow) are oriented to intersect perpendicularly at the apex of the SMRL and are also aligned along the axis of the lateral rectus; B) Same image seen in B without the planes of orientation. The lateral rectus (LR) reaches the SMRL. As if continuing the muscle, a band of tissue, possibly the annulus of Zinn (AZ), crosses the SOF to insert into the body of the sphenoid, at the base of the optic strut; C) Same orbit of A and B. Though still intersecting at the SMRL apex, spatial planes (blue and yellow) have been reoriented along the axis of the inferior rectus; D) Same image seen in C without the planes of orientation. The inferior rectus (IR) seems to reach the SMRL.

syndrome is characterized by ophthalmoplegia, proptosis and ptosis for the involvement of the III, IV and VI cranial nerves, hypoesthesia of the cornea, upper eyelid and ipsilateral forehead for compression of the terminal branches of the ophthalmic nerve, and possible visual impairment from optic neuropathy (Goyal et al., 2018). In many respects, the SOF syndrome is similar to the previous one, but it spares the optic nerve as it is generated by pathologies immediately anterior to the orbital apex (Jin et al., 2018). Cranio-facial traumatic injuries are certainly the most frequent cause of both syndromes. In the fractures of the lateral wall of the orbit, the involvement of structures traversing the region can be particularly severe and may require emergency decompression in the attempt to preserve sight and eye motility (Bun et al., 1996; Imaizumi et al., 2014; Warburton et al., 2016). Both syndromes can also be secondary to neoplasia, infection, aneurysms of the intracavernous internal carotid artery growing anteriorly into the orbit, inflammatory and autoimmune diseases like sarcoidosis, thyroid ophthalmopathy, and granulomatosis with polyangiitis, formerly known as Wegener's granulomatosis (Goyal et al., 2018). It is evident that, in all these conditions, compression can be more severe in the presence of a well-developed SMRL which reduces the room for neurovascular structures. It is also important for the surgeon to be aware of this inconstant but sometime bulky bony variant.

When shown on pre-operative CT images, SMRL can represent an important landmark for surgical approach, especially when neuronavigation is used. SMRL can serve as a reference point in lateral and inferolateral approaches (Maroon and Kennerdell, 1984; Gönül and Timurkaynak, 1999), indicating the insertion of the lateral rectus constantly, and sometimes even the insertion of the inferior rectus

muscle, as well as pointing out the inferior margin of SOF. In image guided surgery with neuronavigation, it can be a reliable reference point for preoperative planning, and it may proof helpful in verifying accuracy of navigation during surgery (Terpolilli et al., 2016; Ali et al., 2017). In orbital reconstruction after fracture or tumor surgery, when normal anatomy is altered, SMRL may represent a key anatomical landmark both in preoperative planning and intraoperatively, for shaping and positioning an orbital mesh (Raveggi et al., 2023).

In this respect, it is relevant to have topographical information to correctly place the SMRL within the orbital apex. First of all, it is interesting to note that the SMRL, in contrast to what has been reported so far (Lang, 1983; Bisaria et al., 1996; Bron et al., 2001; Snell and Lemp, 2016) in most cases is not a feature of the SOF. Admittedly, it is frequently very close to the lower margin of the SOF ($\leq$ 1.5 mm in 61.5% of cases) but it is incorporated into it only in 16.4% of cases. Overall, therefore, the SMRL appears more as a feature of the orbital plate of the sphenoid than of its posterior margin (lower margin of the SOF) and in 38.5% of cases it is located far from the SOF ($>$ 1.5 mm). Secondly, considering the quadrangular shape of the orbital plate of the sphenoid, the SRML is always located in its postero-inferior quadrant at a distance of 1.25 $\pm$ 0.85 mm from the SOF lower margin and 8.5 $\pm$ 4.1 mm from the IOF. The lower standard deviation of the distance from the SOF implies that SMRL placement is more variable on the vertical than on the horizontal axis.

The size of the SMRL is not defined exclusively by its height (though this is certainly the most suggestive feature) but also by its width. This parameter can be roughly evaluated by the angle formed by the two margins converging at the spine apex. Indeed, most of the SMRLs appears relatively large structures as the angle is more frequently obtuse.

Though mostly aligned horizontally, orientation of the SMRLs can be markedly different, even vertical in one orbit. The functional meaning of a different orientation is unknown and can only find an explanation identifying the anatomical structures that take insertion into the spine. In this respect, 3D MPR allowed us to observe that structures running close to the horizontal plane and inserting into SMRLs correspond to the lateral rectus and likely to the tendinous ring. In a way, the SMRL appears as intercalated between the lateral rectus and the annulus of Zinn. Inconstantly, we have also observed a portion of the inferior rectus that seems to point to the SMRL. It is noteworthy to mention that CT shows the annulus of Zinn inserting also into the base of the optic strut, a site that, on dry skulls, shows with a remarkable frequency the presence of a small tubercle that could be interpreted as the attachment site of the tendinous ring. To our knowledge, precise reference points for the attachment of the annulus of Zinn to the bony surface have not been studied so far. Even recent investigations on the topography of the tendinous ring did not focus on its bony insertions, dealing rather with muscle origins from the annulus (Naito et al., 2019; Kim et al., 2020; Lacey et al., 2022). Yet, it is frequently observed that three recti muscles (lateral, inferior and medial recti) originate almost together from the lower part of the annulus with the inferior rectus adjacent laterally and almost fused with the lateral rectus (Naito et al., 2019; Kim et al., 2020; Kanehira et al., 2022). This observation indirectly supports ours on the common, though inconstant, origin of the lateral and inferior recti from that part of the annulus inserting into the SMRL. When present, therefore, the SMRL could be considered a bony landmark for retracing the insertion of the common tendinous ring.

We also investigated whether the SMRL is the result of postnatal development and/or whether the SMRL might grow with time. Indeed, no correlation can be found between spine length and age. The presence of already well-developed SMRLs in fetal skulls, on the other hand, supports the idea that the SMRL is a genetically determined bony variant which likely develops with different modalities because multifactorial and polygenic as many other minor bony variants are (Hauser and De Stefano, 1989).

Funding

This research did not receive any specific grant from funding agencies in the public, commercial, or not-for-profit sectors.

Ethical statement

This retrospective study involving human participants was in accordance with the ethical standards of the institutional and national research committee and with the 1964 Helsinki Declaration and its later amendments or comparable ethical standards. The Regional Ethic Committee for the Clinical Sperimentation of the Tuscany (South-West Vast Area) approved this study (approval number: 24908).

CRediT authorship contribution statement

Eugenio Bertelli provided the study conceptualization and design. Material preparation, data collection and analysis were performed by Denise Bonente, Miriam Durante, Sara Ottolenghi and Sandra Bracco. The first draft of the manuscript was written by Eugenio Bertelli and Denise Bonente; Review and editing were carried out by Claudio Nicoletti and Virginia Barone; Vitaliano Francesco Muzii contributed to the writing of the manuscript and to review it; all authors commented on previous versions of the manuscript. All authors read and approved the final manuscript.

Declaration of Competing Interest

The authors declare that they have no known competing financial interests or personal relationships that could have appeared to influence the work reported in this paper.

References

Ali, M.J., Naik, M.N., Kaliki, S., Dave, T.V., Dendukuri, G., 2017. Interactive navigation-guided ophthalmic plastic surgery: the techniques and utility of 3-dimentional navigation. Can. J. Ophthalmol. 52, 250–257. https://doi.org/10.1016/j.jcjo.2016.10.012.

Bertelli, E., 2014. Metoptic canal, duplication of the optic canal and Warwick's foramen in human orbits. Anat. Sci. Int. 89, 34–45. https://doi.org/10.1007/s12565-013-0197-7.

Bertelli, E., 2019. Anatomy of The Eye and Human Visual System. Piccin Nuova Libraria Padova.

Bertelli, E., Regoli, M., 2014. Branching of the foramen rotundum. A rare variation of the sphenoid. It. J. Anat. Embryol. 119, 148–152.

Bertelli, E., Regoli, M., Bracco, S., 2017. An update on the variations of the orbital blood supply and hemodynamic. Surg. Radiol. Anat. 39, 485–496. https://doi.org/10.1007/s00276-016-1776-9.

Bisaria, K.K., Kumar, N., Prakesh, M., Sharma, P.K., Agarwal, P.P., Bisaria, S.D., Lakhtakia, P.K., Premesagar, I.C., 1996. The lateral rectus spine of the superior orbital fissure. J. Anat. 189, 243–245.

Bracco, S., Gennari, P., Vallone, I.M., Tassi, R., Acampa, M., Martini, G., Bertelli, E., 2016. Double ophthalmic arteries arising from the internal carotid artery. A case report of a hidden second ophthalmic artery. Surg. Radiol. Anat. 38, 1233–1237. https://doi.org/10.1007/s00276-016-1672-3.

Bron, A.J., Tripathi, R.C., Tripathi, B.J., 2001. Wolff's anatomy of the eye and orbit, 8th edition. Arnold,, London.

Bun, R.J., Vissink, R.R., Boss, R.R., 1996. Traumatic superior orbital fissure syndrome: report of two cases. J. Oral. Maxillofac. Surg. 54, 758–761. https://doi.org/10.1016/s0278-2391(96)90698-9.

Gönül, E., Timurkaynak, E., 1999. Inferolateral microsurgical approach to the orbit: an anatomical study. Minim. Invas. Neurosurg. 42, 137–141. https://doi.org/10.1055/s-2008-1053386.

Goyal, P., Lee, S., Gupta, N., Kumar, Y., Mangla, M., Hooda, K., Li, S., Mangla, R., 2018. Orbital apex disorders: Imaging findings and management. Neuroradiol. J. 31, 104–125. https://doi.org/10.1177/1971400917740361.

Hauser, G., De Stefano, G.F., 1989. Epigenetic variants of the human skull. Schweizerbart'sche Verlagsbuchhandlung, Stuttgart,.

Imaizumi, A., Kunihiro, I., Ishikawa, Y., Nakayoshi, I., 2014. Successful treatment of the traumatic orbital apex syndrome due to direct bone compression. Craniomaxillofac. Trauma Reconstr. 7, 318–322. https://doi.org/10.1055/s-0034-1390245.

Jin, H., Gonga, S., Hana, K., Wanga, J., Lva, L., Donga, Y., Zhanga, D., Houa, L., 2018. Clinical management of traumatic superior orbital fissure and orbital apex syndromes. Clin. Neurol. Neurosurg. 165, 50–54. https://doi.org/10.1016/j.clineuro.2017.12.022.

Kanehira, C., Yamamoto, M., Hirouchi, H., Ishizuka, S., Sakiyama, K., Higa, K., Murakami, G., Abe, S., 2022. Tendinous annulus of Zinn for a common origin of the extraocular rectus muscles: a histological study of the orbital apex from donated elderly cadavers. Anat. Sci. Int. 97, 369–379. https://doi.org/10.1007/s12565-022-00649-8.

Kim, J.H., Hayashi, S., Yamamoto, M., Murakami, G., Wilting, J., Rodríguez-Vázquez, J. F., 2020. Examination of the annular tendon (annulus of Zinn) as a common origin of the extraocular rectus muscles: 2. embryological basis of extraocular muscles anomalies. Invest. Ophthalmol. Vis. Sci. 61, 5. https://doi.org/10.1167/iovs.61.12.5.

Lacey, H., Oliphant, H., Smith, C., Koenig, M., Rajak, S., 2022. Topographical anatomy of the annulus of Zinn. Sci. Rep. 12, 1064. https://doi.org/10.1038/s41598-022-05178-y.

Lang, J., 1983. Clinical anatomy of the head. Neurocranium, orbit, craniocervical regions. Soringer-Verlag,, Heidelberg.

Macchi, V., Regoli, M., Bracco, S., Nicoletti, C., Morra, A., Porzionato, A., De Caro, R., Bertelli, E., 2016. Clinical anatomy of the orbitomeningeal foramens: variational anatomy of the canals connecting the orbit with the cranial cavity. Surg. Radiol. Anat. 38, 165–177. https://doi.org/10.1007/s00276-015-1530-8.

Maroon, J.C., Kennerdell, J.S., 1984. Surgical approaches to the orbit. Indications and techniques. J. Neurosurg. 60, 1226–1235. https://doi.org/10.3171/jns.1984.60.6.1226.

Naito, T., Cho, K.H., Yamamoto, M., Hirouchi, H., Murakami, G., Hayashi, S., Abe, S., 2019. Examination of the topographical anatomy and fetal development of the tendinous annulus of Zinn for a common origin of the extraocular recti. Invest. Ophthalmol. Vis. Sci. 60, 4564–4573. https://doi.org/10.1167/iovs.19-28094.

Raveggi, E., Gerbino, G., Autorino, U., Novaresio, A., Ramieri, G., Zavattero, E., 2023. Accuracy of intraoperative navigation for orbital fracture repair: a retrospective morphometric analysis. J. Craniomaxillofac. Surg. 51, 107–116. https://doi.org/10.1016/j.jcms.2023.01.016.

Regoli, M., Bertelli, E., 2017. The revised anatomy of the canals connecting the orbit with the cranial cavity. Orbit 36, 110–117. https://doi.org/10.1080/01676830.2017.1279662.

Snell, R.S., Lemp, M.A., 2016. Clinical Anatomy of the eye. Wiley-Blackwell,, New Delhi.

Snijders, R.J.M., Nicolaides, K.H., 1994. Foetal biometry at 14-40 weeks gestation. Ultrasound Obstet. Gynecol. 4, 34–48. https://doi.org/10.1046/j.1469-0705.1994.04010034.x.

Terpolilli, N.A., Rachinger, W., Kunz, M., Thon, N., Flatz, W.H., Tonn, J.C., Schichor, C., 2016. Orbit-associated tumors: navigation and control of resection using intraoperative computed tomography. J. Neurosurg. 124, 1319–1327. https://doi.org/10.3171/2015.5.JNS15330.

Thane, G.D., 1893. Quain's elements of anatomy. Pt. 1 Osteology. Longmans, Green & Co, London & New York.

Warburton, R.E., Brookes, C.C.D., Golden, B.A., Turvey, T.A., 2016. Orbital apex disorders: a case series. Int. J. Oral. Maxillofac. Surg. 45, 497–506. https://doi.org/10.1016/j.ijom.2015.10.014.